HTML ABSTRACT + LINKS

Photoluminescence studies on Al and Ga interdiffusion across (Al,Ga)Sb/GaSb quantum well interfaces

M. Gonzalez-Debs
Department of Chemical and Biological Engineering, University of Wisconsin–Madison, Madison, Wisconsin 53706

J. G. Cederberg and R. M. Biefeld
Sandia National Laboratories, P.O. Box 5800, Albuquerque, New Mexico 87123-0601

T. F. Kuech[a)]
Department of Chemical and Biological Engineering, University of Wisconsin–Madison, Madison, Wisconsin 53706

(Received 20 January 2005; accepted 13 March 2005; published online 11 May 2005)

The thermal interdiffusion of AlSb/GaSb multiquantum wells was measured and the intrinsic diffusivities of Al and Ga determined over a temperature range of 823–948 K for 30–9000 s. The 77-K photoluminescence (PL) was used to monitor the extent of interdiffusion through the shifts in the superlattice luminescence peaks. The chemical diffusion coefficient was quantitatively determined by fitting the observed PL peak shifts to the solution of the Schrödinger equation, using a potential derived from the solution of the diffusion equation. The value of the interdiffusion coefficient ranged from 5.2×10^{-4} to 0.06 nm^2/s over the conditions studied and was characterized by an activation energy of 3.0 ± 0.1 eV. The intrinsic diffusion coefficients for Al and Ga were also determined with higher values for Al than for Ga, described by activation energies of 2.8 ± 0.4 and 1.1 ± 0.1 eV, respectively. © *2005 American Institute of Physics*. [DOI: 10.1063/1.1900286]

I. INTRODUCTION

Devices using semiconductor heterostructures require detailed consideration of the electronic band-structure design, structural stability, and chemical compatibility of the component layers. The resulting device heterointerfaces are affected by defects within the bulk and at the surface, compositional transitions, and exposure to high temperatures. In the present work, the AlSb/GaSb heterointerface is studied. The near lattice-matched InAs/GaSb/AlSb system is finding use in many quantum structures,[1–3] or as the ternary alloy such as AlGaSb/GaSb.[4] Electronic and optoelectronic heterostructures have been proposed utilizing these materials in hundred gigahertz logic circuits, terahertz transistors, resonant tunneling diodes,[5] infrared lasers, and infrared detectors. These applications are enabled by the unique band alignments within this heterojunction system. Superlattice-based photodetectors have been proposed which allow normal-incidence electronic intersubband transitions.[1,6] Intersubband optical transitions within AlSb/GaSb/InAs quantum well (QW) structures have drawn attention because of their large oscillator strength and the wide tunability over the near- to far-infrared wavelength range.[2] The large difference in the refractive indices between GaSb and AlSb has allowed the design of high reflectivity Bragg reflectors required in vertical-cavity surface-emitting lasers (VCSEL's) used for high-bit rate optical communication.[4]

Controlled compositional transitions across interfaces and the detailed microstructure during growth and processing can determine and limit the device performance. Interdiffusion can lead to shifts in the optical characteristics of devices due to modifications in the electronic band structure after thermal treatments. In electronic devices, initially square quantum wells can acquire graded concentration profiles which can affect the electrical transport across and parallel to the heterointerface. By characterizing the interdiffusion rates, determining the activation energies involved, processing conditions can be adjusted to reach and maintain performance standards for a device structure.

The interdiffusion at (Al,Ga)Sb/GaSb interfaces has not been studied as extensively as that in the arsenide systems such as InGaAs/GaAs,[7,8] AlAs/GaAs,[9] or quaternary material systems such as InGaAs/InP.[10–13] In this paper, diffusion in (Al,Ga)Sb/GaSb multiple quantum well structures was characterized and both the chemical interdiffusion rate of Al and Ga across the interface and the chemical intrinsic diffusivities of Al and Ga were determined using a phenomenological model. Photoluminescence (PL) spectra were measured at 77 K from ten-period (Al,Ga)Sb/GaSb superlattices before and after interdiffusion, which was controlled by rapid thermal annealing the samples at selected temperatures and time periods.

PL is a common technique used in interdiffusion studies. Alternative techniques include Auger electron spectroscopy (AES), x-ray diffraction (XRD),[14] transmission electron microscopy (TEM),[15] secondary-ion-mass spectroscopy (SIMS),[16] and infrared-absorption spectroscopy (or Fourier transform IR).[17] Similar quantum well structures have been used with these techniques, yet some of these methods exhibit considerable limitations. For example, intermixing caused by the sputter erosion in AES measurements can perturb the measured profile. Especially during the early stages

[a)]Electronic mail: kuech@engr.wisc.edu

 © 2005 American Institute of Physics

Downloaded 02 Mar 2007 to 128.104.198.71. Redistribution subject to AIP license or copyright, see http://jap.aip.org/jap/copyright.jsp

TABLE I. Description of (Al,Ga)Sb/GaSb samples used for this study.

Sample	GaSb substrate	Initial Al barrier composition	Well width (nm)	Barrier width (nm)	Growth temp. (K)
1	Te-doped	1	12.9	3.3	823
2	Te-doped	1	13.5	4.4	823
3	undoped	1	13.4	1.9	773
4	undoped	0.6	14.8	2.9	773

of intermixing where the degree of interdiffusion is very small, optical techniques such as PL have demonstrated promising results.[18] Therefore, PL spectra were used for this study to obtain quantitative data at the initial stages of interdiffusion.

Blueshifts in the PL spectra observed after interdiffusion for the first-order electron to heavy-hole transition were fitted to the solution of the Schrödinger equation within an envelop function approximation,[18] using a potential derived from the solution of Fick's second law of diffusion, to quantitatively determine the chemical diffusion coefficients. The expected PL blue energy shift was calculated by adding the confinement energies at the conduction and valence bands with the resulting minimum-energy band gap of the wells. Two models are employed. Model 1 assumes no concentration dependence to the chemical diffusion coefficient. The observed PL blue energy shift at each anneal time period, t, was compared to the calculated shift at each $\tilde{D}t$ to determine the interdiffusion coefficient, $\tilde{D}$. Within model 2, the concentration dependence was included by relating $\tilde{D}$ to the aluminum composition (cation mole fraction), c, and intrinsic diffusion coefficients of the species involved (D_{Al} and D_{Ga}) by following Darken's analysis,[19] such that,

$$\tilde{D} = D_{\mathrm{Al}}(1-c) + D_{\mathrm{Ga}}(c). \tag{1}$$

Thus, three diffusion coefficients, $\tilde{D}, D_{\mathrm{Al}}$, and D_{Ga}, were determined for each temperature studied. Models 1 and 2 were used to determine the extent of the concentration dependence to $\tilde{D}$ and determine the Arrhenius parameters for the interdiffusion and intrinsic diffusion of Al and Ga.

II. METHODOLOGY

A. Experiment

The structures analyzed for this study consist of ten-period multiple quantum wells of GaSb films separated by either AlSb (samples 1–3) or $Al_{0.6}Ga_{0.4}Sb$ barriers (sample 4). The sample descriptions are summarized in Table I. The substrate material was GaSb(100) with a miscut of 6° toward the nearest (111)B direction. GaSb well layers ranged between 12.9 and 14.8 nm thick, while barrier regions ranged between 1.9 and 4.4 nm thick, as determined from growth calibrations and verified through x-ray diffraction measurements. To prevent the surface Al oxidation, a GaSb top layer was grown on all samples. All samples described in Table I were grown by metal-organic vapor phase epitaxy (MOVPE) at 823 K (samples 1 and 2) or 773 K (samples 3 and 4) and capped with a 100-nm plasma-deposited SiN_x layer grown at 523 K and 40 mTorr. The SiN_x capping layer prevents Sb sublimation during the thermal anneals. Samples were cleaved into multiple pieces each with the dimensions of 1×0.5 cm^2. These pieces were thermally annealed at selected temperatures from 823 to 948 K and times ranging from 30 to 9000 s. Samples were annealed in a graphite crucible on a Si wafer with the SiN_x cap facing upwards, at a pressure of 200 mbar in a N_2 atmosphere. Photoluminescence spectra before and after the thermal anneals were measured at 77 K by immersion in liquid nitrogen. The PL excitation source was a 780-nm diode laser. The beam was focused on the sample using a fiber optic and the resulting PL was filtered using a double-sided polished GaAs wafer. PL was detected using an InGaAs extended wavelength detector with a 1.7-μm wavelength cutoff. X-ray diffraction rocking curve measurements were carried out on both the annealed and as-grown samples to determine the period length, barrier and well widths, and average composition. Rocking curves were simulated using commercial dynamical simulation software.

B. PL model development

The interdiffusion of Al and Ga across the (Al,Ga)Sb/GaSb interfaces was characterized by studying the changes in confinement energy within the wells as a function of time and temperature. Quantum-mechanical wave-function calculations were performed to model the interband transition energy shifts resulting from the changes in well geometry after annealing. Two different algorithms were written to calculate the expected PL energy shifts. Both models solve Fick's second law of diffusion along with Schrödinger's equation to determine the quantum confinement within the wells. The one-dimensional time-independent Schrödinger's wave equation is

$$\left[-\frac{\hbar^2}{2m^*}\frac{d^2}{dx^2} + V(x)\right]\psi_n(x) = E_n\psi_n(x), \tag{2}$$

where E_n and $\psi_n(x)$ are the total energy and wave function, respectively, corresponding to the nth state of the particle under study (e.g., electron, heavy hole, or light hole), m^* is the effective mass of the particle, and $\hbar$ is Planck's constant. The effective masses used were the composition-averaged values from GaSb and AlSb effective masses.[20] The potential profile $V(x)$ was represented as a periodic function expanded as a Fourier series in the reciprocal-lattice vectors, G, having the form:[21]

$$V(x) = \sum_G V_G e^{iGx},$$

where

Downloaded 02 Mar 2007 to 128.104.198.71. Redistribution subject to AIP license or copyright, see http://jap.aip.org/jap/copyright.jsp

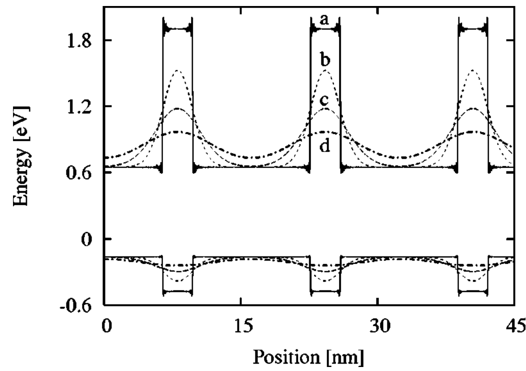

FIG. 1. Potential profile for the interdiffusion of an AlSb/GaSb quantum well structure at (a) $\tilde{D}t=0\ \text{nm}^2$, (b) $\tilde{D}t=1\ \text{nm}^2$, (c) $\tilde{D}t=3\ \text{nm}^2$, and (d) $\tilde{D}t=8\ \text{nm}^2$.

$$G=\frac{2\pi\mu}{L}, \tag{3}$$

where G is evaluated for all values of index μ, i.e., $-\infty<\mu<\infty$. The coefficients V_G were obtained by evaluating the following integral:

$$V_G=\frac{1}{L}\int_{-L/2}^{L/2}\Delta E_g(x,\tilde{D}t)e^{iGx}dx, \tag{4}$$

where L is the sum of the well width, a, and barrier width, b, and $\Delta E_g(x,\tilde{D}t)$ is the potential well determined by subtracting the resulting energy gap at $x=0$ from the same at any x, i.e., $\Delta E_g(x,\tilde{D}t)=E_g(x,\tilde{D}t)-E_g(0,\tilde{D}t)$. The resulting local band gap, which is associated with the AlGaSb formed after interdiffusion, is a function of x and $\tilde{D}t$ through its concentration dependence,

$$E_g[c(x,\tilde{D}t)]=E_{\text{AlSb}}c(x,\tilde{D}t)+E_{\text{GaSb}}[1-c(x,\tilde{D}t)] - E_B c(x,\tilde{D}t)[1-c(x,\tilde{D}t)], \tag{5}$$

where a temperature-independent bowing coefficient, E_B, of 0.47 eV (Ref. 22) was used. E_{AlSb} and E_{GaSb} are the energy band gaps of AlSb and GaSb calculated at 77 K from Varshni parameters.[20] Figure 1 shows the valence and conduction energy bands for an AlSb/GaSb superlattice as a function of position at different values of $\tilde{D}t$, assigning 80% of the total band-gap discontinuity to the conduction band,[22] assuming $\tilde{D}$ is composition independent. This plot depicts the changes in the potential profile as the interdiffusion proceeds. As $\tilde{D}t$ is increased, the profile becomes less square with substantial grading of the quantum well. All QW's were assumed to interdiffuse at the same rate.

The two models differ in the generation of the concentration profile used to determine the potential. Model 1 used an analytical solution to Fick's second law by assuming an interdiffusion coefficient independent of concentration, $\tilde{D}$,

$$c(x,t)=\frac{1}{L}(aC_1+bC_2) + \sum_{\mu=1}^{\infty}\frac{2(C_1-C_2)}{\pi\mu}\sin\left(\frac{\pi\mu a}{L}\right)\cos\left(\frac{2\pi\mu x}{L}\right)e^{-(2\pi\mu/L)^2\tilde{D}t}, \tag{6}$$

while model 2 numerically solved Fick's second law of diffusion for discrete values of concentration using Darken's equation [Eq. (1)] to relate a concentration-dependent interdiffusion coefficient $\tilde{D}(c)$ to the intrinsic diffusion coefficients of Al in GaSb (D_{Al}) and Ga in AlSb (D_{Ga}). In model 2, Fick's second law equation was solved using the forward time-centered space (FTCS) representation to calculate the composition profiles.[23] The energy-band potential profiles were then determined from these composition profiles, transformed into a Fourier series, and used to solve for the eigenvalues of the Schrödinger equation. The wave function $\psi_n(x)$ was expanded into plane waves as $\psi_n(x)=\Sigma_k B(k)e^{ikx}$, where k is a real function of integer, n, $k=2\pi n/L$. The wave equation resulting from the substitution of both series, $\psi_n(x)$ and the potential-energy profile $V(x)$, into Eq. (2) is[21]

$$\sum_k \frac{\hbar^2}{2m^*}k^2B(k)e^{ikx}+\sum_G\sum_k V_G B(k)e^{i(k+G)x} = E_n\sum_k B(k)e^{ikx}. \tag{7}$$

Confinement energies for the conduction and valence bands were obtained from the eigenvalues solved for the respective particle evaluated. The plane-wave basis set was truncated at 101. The eigenvalue solutions were obtained and ordered, taking the smallest value, E_0, as the interband transition level observable through PL. The expected PL energy, E_{PL}, is therefore,

$$E_{\text{PL}}=E_{0,e}+E_g+E_{0,h}-E_{\text{exc}}, \tag{8}$$

where subscripts e and h denote the conduction- and valence-band confinement energies. E_{exc} accounts for the exciton binding energy, estimated using a hydrogenic model.[24]

For model 1, an interdiffusion coefficient was determined for each anneal through fitting the experimental PL peak shift to the expected shifts as a function of $\tilde{D}t$, since the diffusion time is known. Subsequently, the Arrhenius temperature dependence of the interdiffusion coefficient was used to determine the activation energy and preexponential factor of Al and Ga in the (Al,Ga)Sb/GaSb material system. For model 2, the experimental PL shifts were compared to calculated PL shifts at various combinations of Ga diffusivities (D_{Ga}) and Al and Ga diffusivity ratios ($r=D_{\text{Al}}/D_{\text{Ga}}$) to determine the most probable values at each temperature and obtain the activation energy and preexponential factors.

The Kronig–Penney model was used to generate analytical solutions to the multi-QW/superlattice structure at the initial conditions, i.e., $\tilde{D}t=0$, for the problem at hand.[25]

Downloaded 02 Mar 2007 to 128.104.198.71. Redistribution subject to AIP license or copyright, see http://jap.aip.org/jap/copyright.jsp

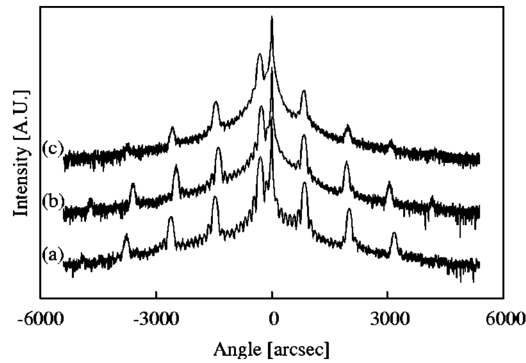

FIG. 2. X-ray diffraction measurements for AlSb/GaSb superlattice sample 1 (a) as-grown and postannealed at 848 K for (b) 1250 s and (c) 5000 s.

III. RESULTS

All structures used for this project were grown below their critical thickness according to superlattice strain criteria reported by Houghton *et al.*,[26] in order to prevent the formation of misfit dislocations at the interfaces. Threading dislocations can act as a diffusion "pipe" with a high local diffusivity. Similarly, diffusional processes can affect the dislocation generation, particularly in highly strained systems. Samples below the critical thickness were therefore used to eliminate the possibility of additional energy (i.e., extended defect-related) levels within the band gap and their associated recombination paths which would affect the PL measurement interpretation.

Before annealing, XRD rocking curves were obtained at four points along the radius to verify the uniformity across the grown wafer. Also, XRD spectra were collected to study the structural changes resulting from the interdiffusion. The XRD spectra, shown on Fig. 2, depict three rocking curves obtained from the as-grown samples, and after two different annealing treatments. Simulation software was used to determine the thickness and mean composition of the layers, considering the substrate 6° miscut.

The line shapes in Fig. 2 indicate a loss of intensity in the superlattice peaks, associated with the interdiffusion process. However, the overall peak structure indicates that no substantial defect introduction has occurred. As observed by Bocchi *et al.*, it is not possible, in principle, to distinguish between compositionally graded interfaces and well thicknesses fluctuations with XRD.[27] The initial planar interface and the high degree of uniformity within the wafer support the loss of satellite intensity as being due to the compositional grading due to thermal annealing. This ambiguity motivates the use of PL to monitor the interdiffusion process.

The PL spectra taken at 77 K for AlSb/GaSb superlattices before and after annealing at 908 K for 125 s are shown for samples 1 and 3 in Figs. 3(a) and 3(b), respectively. Both figures show a blue peak shift only for the high-energy peak, which is attributed to the interband-to-interband direct recombination within the quantum well. In Fig. 3(a), the peak at lower energy, $\lambda \sim 1660$ nm, has been attributed to the Ga_{Sb} acceptor to conduction-band transition.[28,29] In Fig. 3(b), the peaks at lower energy, $\lambda \sim 1551$ and 1598 nm, are attributed to substrate band-to-band recombination (1551 nm) and to transitions of free electrons to neutral native acceptors (1598

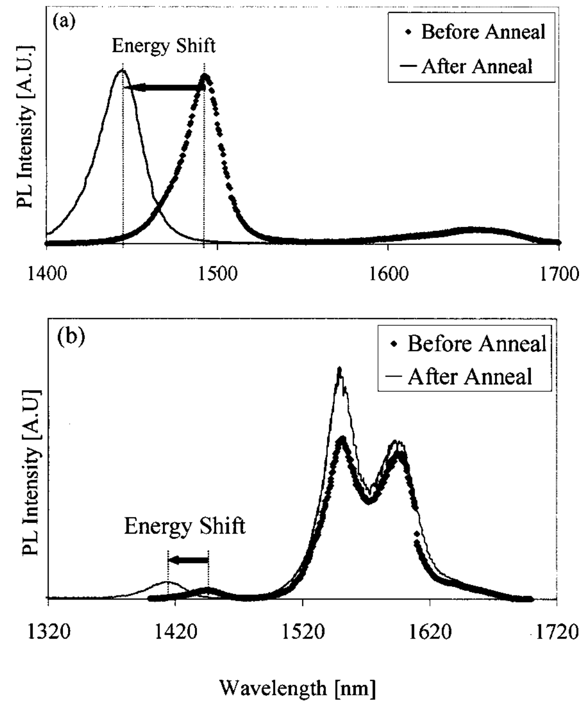

FIG. 3. Photoluminescence spectra at 77 K for (a) sample 1 and (b) sample 3 consisting of AlSb barriers and GaSb wells, before and after annealing at 908 K for 125 s.

nm).[30] Agert *et al.* have also attributed the 1551-nm PL peak to transitions of free electrons to unspecified neutral acceptors, and have reported this wavelength for recombination of excitons bound to an unspecified acceptor for Si-doped GaSb spectra taken at 4.2 K.[30] However, the data presented here were observed at 77 K, at which the probability of having significant excitonic emissions is reduced.

PL intensity ratios between the superlattice- and substrate-assigned peaks vary from samples 1 and 2, with respect to samples 3 and 4. Samples 3 and 4 had a thicker GaSb cap which attenuated the superlattice emission. Additionally, improved optical emission for heterostructure samples with Te-doped substrates (1 and 2) instead of undoped GaSb (3 and 4) has been previously observed.[31]

PL spectra from sample 4 annealed at 848 K for long-time periods (>5000 s) lacked the high-energy superlattice peak. Sample 4 had (Al,Ga)Sb barriers prior to the anneals, having a lower barrier band gap than the other samples studied which had AlSb barriers initially. In this sample, the lower Al composition barriers lead to a decreased well depth. Upon sufficient annealing and hence interdiffusion, carrier confinement was lost and the PL emission was no longer observed. Figure 4 presents the expected PL energy for AlSb/GaSb superlattices, denoted as E_{PL} in Eq. (8), as a function of $\tilde{D}t$. For extended diffusion conditions, i.e., high $\tilde{D}t$ values, the expected PL energy converges to the value of the (Al,Ga)Sb for the compositionally homogenized structure.

For Figs. 3(a) and 3(b), the higher-energy peaks exhibit an energy shift of 29 and 21 meV, respectively, after annealing. The blue energy shift for this peak was closely monitored for all samples after annealing at selected temperatures

Downloaded 02 Mar 2007 to 128.104.198.71. Redistribution subject to AIP license or copyright, see http://jap.aip.org/jap/copyright.jsp

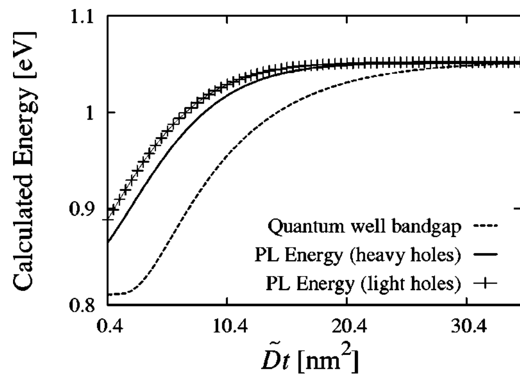

FIG. 4. Expected PL energies as a function of $\tilde{D}t$, calculated as shown in Eq. (8) using confinement energies from model 1. Expected PL energies were evaluated considering heavy holes ($E_{0,h}=E_{0,\mathrm{hh}}$) and light holes ($E_{0,h}=E_{0,\mathrm{lh}}$) for the calculation of the valence-band confinement energies. Also, the expected quantum well band gap, E_g, is plotted as a dotted line.

and time periods in order to study the changes in band gap and confinement energy of the quantum wells as the interdiffusion progressed. Experimental energy shifts are shown in Fig. 5 as a function of annealing time. As temperatures were raised, larger energy shifts were obtained for shorter annealing times. The linear behavior, observed for annealing times lower than 5000 s, showed identical slopes for different samples annealed at the same temperature, i.e., subsamples from samples 1 and 2 at 948 K exhibited the same slope. At annealing times higher than 5000 s at low temperatures, the energy shifts followed an approximately logarithmic behavior.

Additionally, PL spectra for samples 1 and 2 annealed at 948 K for time periods longer than 250 s included additional, unassigned peaks which may be due to the Al interdiffusion and defect introduction into the quantum wells. These peaks may be due to the indirect edge carrier recombination occurring at band edges such as the L edge, $k=(111)$, rather than the Γ edge, $k=(000)$ which would be expected from our calculation of the interdiffusion. The average compositions of samples 1 and 2 are $c=0.20$ and 0.24, which are close to the direct-to-indirect crossover at $Al_{0.21}Ga_{0.79}Sb$.[32] The PL energy shifts obtained from these peaks therefore did not follow the 948K line, as shown in Fig. 5, which is based on direct-gap emission.

Samples annealed at 873 K were reannealed, doubling the initial anneal time, and compared to other samples annealed at the same temperature and total time. The energy shifts were the same for the annealed and reannealed samples, indicating that the annealing effect is cumulative and the effect of the heating and cooling transients is insignificant.

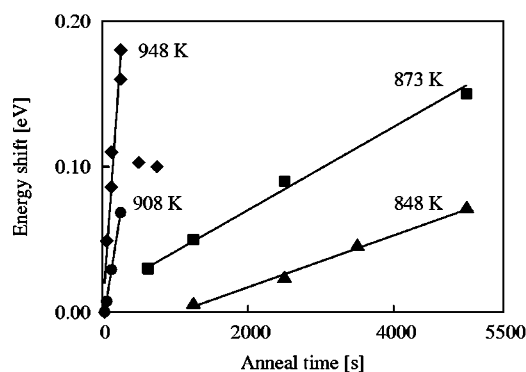

FIG. 5. Energy shifts in photoluminescence spectra after annealing at 948 K (♦), 908 K (●), 873 K (■), and 848 K (▲) at selected time periods.

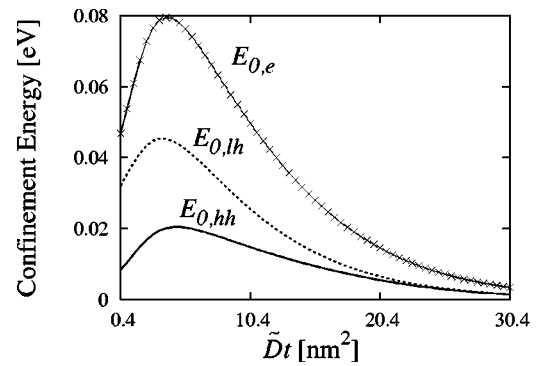

FIG. 6. Calculated confinement energies for electrons ($E_{0,e}$), light holes ($E_{0,\mathrm{lh}}$), and heavy holes ($E_{0,\mathrm{hh}}$) as a function of $\tilde{D}t$ determined using model 1.

IV. DATA ANALYSIS AND DISCUSSION

A. Determining $\tilde{D}$ using model 1

Confinement energies at the conduction ($E_{0,e}$) and valence ($E_{0,lh}$ and $E_{0,hh}$) band were calculated using model 1 and are plotted in Fig. 6 as a function of the product of the interdiffusion coefficient and annealing time, $\tilde{D}t$. The electron- and heavy-hole confinement energies were added using Eq. (8) to determine the total expected PL energies as a function of $\tilde{D}t$, assuming a concentration-independent interdiffusion coefficient. The calculated PL energy shifts, plotted as a line in Fig. 7 as a function of $\tilde{D}t$, were calculated considering the heavy holes for the valence-band confinement energy. The heavy-hole band yields lower emission energies which would be those observed in the PL measurements. These shifts represent the increase in the confinement energy within the wells after the interdiffusion compared to the energy of an initial undiffused well due to the narrowing

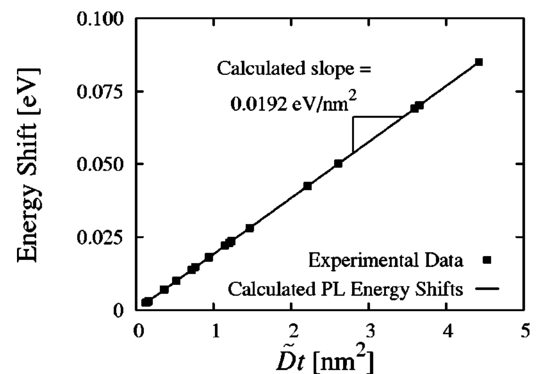

FIG. 7. Experimental and calculated energy shifts as a function of $\tilde{D}t$. The calculated energy shifts were determined by subtracting the expected PL energy for an unannealed sample (at $\tilde{D}t=0$, determined using the Kronig–Penney model) from the expected PL energy calculated using model 1.

Downloaded 02 Mar 2007 to 128.104.198.71. Redistribution subject to AIP license or copyright, see http://jap.aip.org/jap/copyright.jsp

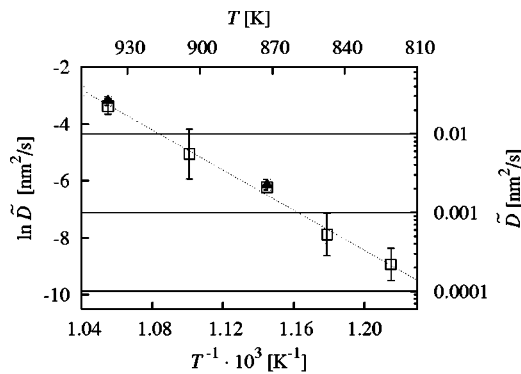

FIG. 8. Arrhenius plot of $\ln(\tilde{D})=-Q(1/k_BT)+\ln(D_0)$ for each calculated $\tilde{D}$ at selected temperatures for samples 1 (white squares) and 2 (black triangles).

of the QW bottom. For the experimentally studied $\tilde{D}t$ range, the energy shifts exhibit a nearly linear behavior. The slope of this line was calculated, using model 1, to be $0.0192\ \mathrm{eV/nm^2}$ for sample 1, for the $\tilde{D}t$ range of $0.4-4.4\ \mathrm{nm}^2$. The experimental PL energy shifts as a function of annealing time (Fig. 5) were compared to the calculated PL energy shifts as a function of $\tilde{D}t$. These calculated PL energy shifts show a linear behavior at low values of $\tilde{D}t$, i.e., less than $4.4\ \mathrm{nm}^2$. As $\tilde{D}t$ is increased, the PL energy shifts behave logarithmically, asymptotically approaching the band-gap energy of the homogenized structure. This value was not reached experimentally since the well composition of the interdiffused structure passes through the Γ-L crossover point leading to an indirect well material.[32] The experimental data used in our analysis are restricted to quantum well compositions below the direct-to-indirect crossover. The crossover between the total emission energy for the direct (Γ) and indirect (L) bands, using heavy-hole masses for the lowest-energy calculations, was calculated using model 1 to be at a $\tilde{D}t$ value of $15.9\ \mathrm{nm}^2$ for this material system for samples 1 and 2.

Fitting the experimental energy shifts to the calculated slope shown in Fig. 7, a value of $\tilde{D}$ was determined for each anneal. The $\tilde{D}$ values were then plotted for each temperature following the Arrhenius equation $\tilde{D}=D_0e^{(-Q/k_BT)}$, as shown in Fig. 8, to determine an overall activation energy Q for the Al and Ga interdiffusion of 3.0 ± 0.1 eV and a preexponential factor of $5(+8/-2)\ \mathrm{cm^2/s}$ for samples 1 and 2. Similarly analyzed, samples 3 and 4 exhibited an activation energy of 2.7 ± 0.1 and 2.4 ± 0.2 eV with a preexponential factor of $0.13(+0.2/-0.08)\ \mathrm{cm^2/s}$ and $2.7\times10^{-3}(+0.05/-0.0)\ \mathrm{cm^2/s}$, respectively.

These AlSb/GaSb interdiffusion coefficient parameters determined from samples 1–3 are comparable to those found in related material systems. Our activation energies are similar to the $In_{0.2}Ga_{0.8}As/GaAs$ (3.9 eV) (Ref. 33) and AlGaAs/GaAs (4.0 eV) (Ref. 9) systems. Reported preexponential factor values ranged from 0.3 to $6\ \mathrm{cm^2/s}$, respectively, again similar to those reported here. For sample 4, which has AlGaSb barriers, the activation energy was slightly lower (2.4 ± 0.2 eV) and the preexponential factor

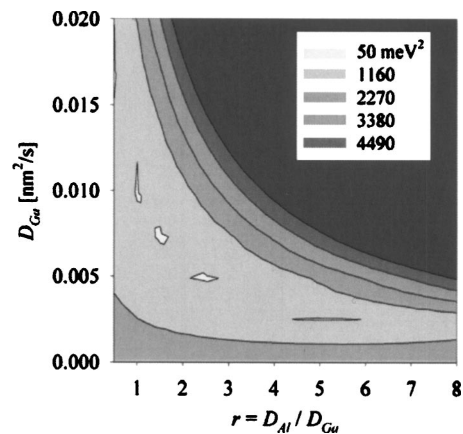

FIG. 9. Contour plot of the χ^2 variance as a function of D_{Ga} and r for sample 3 at 908 K. The 50-meV^2 contour includes a confidence coefficient of $(1-\alpha)=0.5$. The confidence level indicates that with repeated experiments, $(1-\alpha)$ 100% of the cases will give D_{Ga} and r values with variances within this defined contour region. Contours up to 1160 meV^2 represent a confidence level of 90%. Similarly, contours up to 4600 meV^2 include 95%.

was considerably lower than that obtained for AlSb barriers samples, suggesting a concentration-dependent interdiffusion coefficient.

B. Determining D_{Ga} and D_{Al} using model 2

The composition dependence of the interdiffusion coefficient for this material system was considered using model 2. Samples 3 and 4, which are heterostructures with different barrier compositions but grown on similarly undoped substrates, were used to fit the experimental PL shifts to this composition-dependent model. To determine the separate effects of the Al and Ga diffusion, as characterized by their intrinsic diffusion coefficients, the PL energy shifts were compared to expected energy shifts according to model 2. A variance was defined as the sum of the squared difference between experimental and calculated PL energy shifts.[34,35] Contour plots of this variance were constructed as a function of D_{Ga} and $r(r=D_{\mathrm{Al}}/D_{\mathrm{Ga}})$ at 848, 908, and 948 K. Figure 9 shows the contour plot of the variance at 908 K for sample 3. Local and global minima of the variance, $\chi^2(D_{\mathrm{Ga}},r)$, were determined for each sample at all temperatures studied. Figure 10 shows only these minima for two of the three tem-

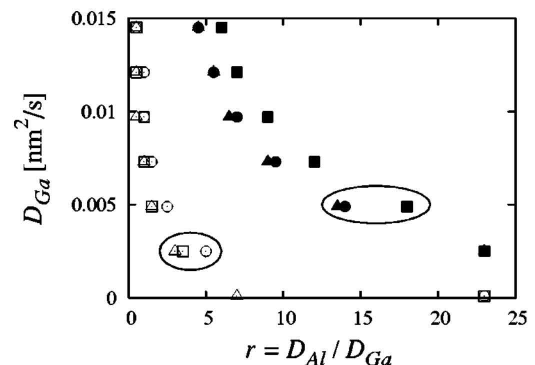

FIG. 10. Local and global minima of the variance for values of D_{Ga} at different r. Contours are omitted for clarity. Calculations were done at 908 K (white markers) and 948 K (black markers) for samples 1 and 2 (triangles), 3 (circles), and 4 (squares). Global minima are encircled.

Downloaded 02 Mar 2007 to 128.104.198.71. Redistribution subject to AIP license or copyright, see http://jap.aip.org/jap/copyright.jsp

peratures studied, the global minima represented by the encircled symbols. At the global minima, the error between PL energy values from model 2 and the experimental data had an average of 34 meV for sample 3, with a 90% confidence level.

D_{Ga} and D_{Al} values were obtained from the global minima. The highest intrinsic diffusivities obtained using model 2 did not necessarily pertain to the sample with the highest initial Al composition, as can be observed in Fig. 10. This result suggests that the interdiffusion coefficient can be derived using the explicit concentration dependence of Darken's analysis within our experimental error. The Arrhenius parameters for these intrinsic diffusivities were determined from the data gathered from all four samples. From the linearization of the Arrhenius equation, the aluminum intrinsic diffusion in GaSb, D_{Al} was characterized by an activation energy of 2.8 ± 0.4 eV and a preexponential factor of $0.82(+100/-0.8)$ cm^2/s. Similarly, the parameters obtained for the gallium intrinsic diffusivity in AlSb, D_{Ga}, were 1.1 ± 0.1 eV as the activation energy, with a preexponential factor of $3(+4/-2)\times10^{-11}$ cm^2/s. Jahnen *et al.*[15] have reported values of intrinsic diffusion coefficients for Al and Ga in AlGaSb at 913 K which agree well with the parameters reported here. They reported a larger diffusivity for Al, having D_{Al} equal to 3×10^{-16} cm^2/s and D_{Ga} between 1×10^{-17} and 4×10^{-18} cm^2/s at 913 K. Using the Arrhenius parameters determined here using model 2, a D_{Al} of 2×10^{-16} cm^2/s and a D_{Ga} of 3×10^{-17} cm^2/s are calculated, showing close quantitative agreement with this previous datum.

The comparison of models 1 and 2 for the data obtained for samples 3 and 4, which assumes that the Al and Ga intrinsic diffusion coefficients are independent of Al composition, leads to the conclusion that concentration dependence of the interdiffusion coefficient is not negligible.

It should be noted that samples 1–3 should possess the same interdiffusion parameters. The difference between sample 1/2 and sample 3 lies in the substrate used for growth. Given the temperature of growth all samples would be intrinsic during the growth process. The defect concentration within the substrate can be different and dependent on the doping through an interaction of the Fermi level with the charged defects, e.g., vacancies. While at high-temperature equilibrium, the doping in the substrate should have little or no effect on the defect concentration within the growing layer. This result, outside of experimental error, may indicate that a possible gradient in the type of defects between the substrate and growing layer may influence the resulting diffusion process. It would be a change in the type of defect present that would give rise to the variation in activation energy.

V. SUMMARY

Al and Ga interdiffusion across (Al,Ga)Sb/GaSb quantum well interfaces has been studied. A significant concentration dependence to the interdiffusion was determined for this diffusion couple over a broad range of diffusion conditions. The values of the activation energies for the interdiffusion coefficients agree well with other material systems which have been described through a vacancy-driven diffusion mechanism.

ACKNOWLEDGMENTS

The authors would like to thank Sandia National Laboratories technical staff for their assistance growing the samples, especially Dr. F. H. Kaatz. One of the authors (M.G.-D.) would also like to acknowledge Yuri W. Ramirez for statistical analysis assistance and Mary Jo Biddy and Yannis Pappas for coding suggestions. Sandia is a multiprogram laboratory operated by Sandia Corporation, a Lockheed Martin Company, for the United States Department of Energy's National Nuclear Security Administration under Contract No. DE-AC0494AL85000.

[1] M. Razeghi, H. Mohseni, and G. J. Brown, J. Korean Phys. Soc. **39**, S257 (2001).
[2] K. Ohtani, Rec. Electr. Commun. Eng. Conversazione Tohoku Univ. **68**, 46 (1999).
[3] P. D. Moran, D. Chow, A. Hunter, and T. F. Kuech, Appl. Phys. Lett. **78**, 2232 (2001).
[4] J. Koeth, R. Dietrich, and A. Forchel, Appl. Phys. Lett. **72**, 1638 (1998).
[5] H. Kitabayashi, T. Waho, and M. Yamamoto, Appl. Phys. Lett. **71**, 512 (1997).
[6] X. Marcadet, I. Prevot, C. Becker, O. Durand, R. Bisaro, F. H. Julien, B. Vinter, and C. Sirtori, Proc. SPIE **4287**, 23 (2001).
[7] W. P. Gillin, D. J. Dunstan, K. P. Homewood, L. K. Howard, and B. J. Sealy, J. Appl. Phys. **73**, 3782 (1993).
[8] P. Melman, E. S. Koteles, B. Elman, and C. A. Armiento, Opt. Quantum Electron. **23**, S981 (1991).
[9] J.-C. Lee and T. E. Schlesinger, J. Vac. Sci. Technol. B **5**, 1187 (1987).
[10] S.-W. Ryu and B.-D. Choe, Appl. Phys. Lett. **71**, 1670 (1997).
[11] F. Bollet, W. P. Gillin, M. Hopkinson, and R. Gwilliam, J. Appl. Phys. **93**, 3881 (2003).
[12] R. M. Cohen, J. Appl. Phys. **73**, 4903 (1993).
[13] T. Fujii, M. Sugawara, S. Yamazaki, and K. Nakajima, J. Cryst. Growth **105**, 348 (1990).
[14] W.-H. Wang, H. Y. Bai, M. Zhang, J. H. Zhao, X. Y. Zhang, W. K. Wang, Phys. Rev. B **59**, 10811 (1999).
[15] B. Jahnen, M. Luysberg, K. Urban, H. Bracht, R. Schmidt, C. Ungermanns, and T. Bleuel, Paper presented at Microscopy Semiconductor Material Conference, 2001 (unpublished), p. 205.
[16] H. Bracht, S. P. Nicols, E. E. Haller, J. P. Silveira, and F. Briones, J. Appl. Phys. **89**, 5393 (2001).
[17] H. Ono, N. Ikarashi, and T. Baba, Appl. Phys. Lett. **66**, 601 (1995).
[18] T. E. Schlesinger and T. F. Kuech, Appl. Phys. Lett. **49**, 519 (1986).
[19] B. Tuck, *Introduction to Diffusion in Semiconductors* (Peter Peregrinus Ltd., Stevenage Herts, England, 1974), p. 116.
[20] I. Vurgaftman, J. R. Meyer, and L. R. Ram-Mohan, J. Appl. Phys. **89**, 5815 (2001).
[21] C. Kittel, *Introduction to Solid State Physics*, 7th ed. (Wiley New York, 1996), p. 183.
[22] C. Alibert, A. Joullie, A. M. Joullie, and C. Ance, Phys. Rev. B **27**, 4946 (1983).
[23] W. H. Press, S. A. Teukolsky, W. T. Vetterling, and B. P. Flannery, *Numerical Recipes in Fortran*, 2nd ed. (Cambridge University Press, New York, 1992), p. 838.
[24] H. Ibach and H. Luth, *Solid-State Physics* (Springer, Berlin, 1991), p. 337.
[25] E. Anderson, *Modern Physics and Quantum Mechanics* (W.B. Saunders Company, Philadelphia, 1971), p. 174.
[26] D. C. Houghton, M. Davies, and M. Dion, Appl. Phys. Lett. **64**, 505 (1994).
[27] C. Bocchi, L. Lazzarini, M. Minelli, and L. Nasi, J. Appl. Phys. **96**, 3110 (2004).
[28] M. Hakala, M. J. Puska, and R. M. Nieminen, J. Appl. Phys. **91**, 4988 (2002).
[29] C. C. Ling, M. K. Lui, S. K. Ma, X. D. Chen, S. Fung, and C. D. Beling, Appl. Phys. Lett. **85**, 384 (2004).

Downloaded 02 Mar 2007 to 128.104.198.71. Redistribution subject to AIP license or copyright, see http://jap.aip.org/jap/copyright.jsp

[30] C. Agert, P. S. Gladkov, and A. W. Bett, Semicond. Sci. Technol. **17**, 39 (2001).
[31] C. A. Wang (private communication).
[32] J. Allegre, M. Averous, and A. Joullie, J. Lumin. **17**, 301 (1978).
[33] S.-W. Ryu, I. Kim, B.-D. Choe, and W. G. Jeong, Appl. Phys. Lett. **67**, 1417 (1995).
[34] P. R. Bevington and D. K. Robinson, *Data Reduction and Error Analysis for the Physical Sciences*, 3rd ed. (McGraw-Hill, New York, 2003), p. 194.
[35] J. Neter, W. Wasserman, and M. H. Kutner, *Applied Linear Statistical Models* (Richard D. Irwin, Inc., Homewood, Illinois, 1985), p. 1078.

Downloaded 02 Mar 2007 to 128.104.198.71. Redistribution subject to AIP license or copyright, see http://jap.aip.org/jap/copyright.jsp